Am J Physiol Heart Circ Physiol 282: H2190–H2197, 2002.
First published Febuary 7, 2002; 10.1152/ajpheart.00759.2001.

Heart size-independent analysis of myocardial function in murine pressure overload hypertrophy

HIDEYUKI TAKAOKA,[1] GIOVANNI ESPOSITO,[1] LAN MAO,[1]
HIROYUKI SUGA,[2] AND HOWARD A. ROCKMAN[1]
[1]*Department of Medicine, Duke University Medical Center, Durham, North Carolina 27710; and* [2]*National Cardiovascular Center Research Institute, Osaka 565-8565, Japan*

Received 23 August 2001; accepted in final form 5 February 2002

Takaoka, Hideyuki, Giovanni Esposito, Lan Mao, Hiroyuki Suga, and Howard A. Rockman. Heart size-independent analysis of myocardial function in murine pressure overload hypertrophy. *Am J Physiol Heart Circ Physiol* 282: H2190–H2197, 2002. First published Febuary 7, 2002; 10.1152/ajpheart.00759.2001.—Pressure overload cardiac hypertrophy may be a compensatory mechanism to normalize systolic wall stress and preserve left ventricular (LV) function. To test this concept, we developed a novel in vivo method to measure myocardial stress (σ)-strain (ε) relations in normal and hypertrophied mice. LV volume was measured using two pairs of miniature omnidirectional piezoelectric crystals implanted orthogonally in the endocardium and one crystal placed on the anterior free wall to measure instantaneous wall thickness. Highly linear σ-ε relations were obtained in control ($n = 7$) and hypertrophied mice produced by 7 days of transverse aortic constriction (TAC; $n = 13$). Administration of dobutamine in control mice significantly increased the load-independent measure of LV contractility, systolic myocardial stiffness. In TAC mice, systolic myocardial stiffness was significantly greater than in control mice (3,156 ± 1,433 vs. 1,435 ± 467 g/cm², $P < 0.01$), indicating enhanced myocardial contractility with pressure overload. However, despite the increased systolic performance, both active (time constant of LV pressure decay) and passive (diastolic myocardial stiffness constant) diastolic properties were markedly abnormal in TAC mice compared with control mice. These data suggest that the development of cardiac hypertrophy is associated with a heightened contractile state, perhaps as an early compensatory response to pressure overload.

systolic myocardial stiffness; contractility; cardiac mechanics; transgenic mice

CARDIAC HYPERTROPHY has long been thought to be a compensatory mechanism of the heart to increased hemodynamic load. Following Laplace's law, the left ventricle (LV) hypertrophies to normalize systolic wall stress by adding sarcomeres in parallel without increasing the number of cells (9). Whereas some studies have suggested that the adapted pressure-overloaded ventricle can maintain a normal myocardial inotropic state (21), others have shown that the hypertrophied ventricle has diminished contractility (5), particularly at increased heart rates (14). The ability to apply a rigorous evaluation of cardiac mechanics to genetically altered mice with impaired (2) or exaggerated (1) hypertrophic responses would be a powerful approach to address whether cardiac hypertrophy plays a role in maintaining cardiac function.

The optimal method to measure cardiac contractile function in the mouse is a matter of some debate. While the slope of the end-systolic pressure-volume (P-V) relation (E'_{max}) is a sensitive measure of LV contractility independent of the loading conditions (23, 24), it is still influenced by heart size. Using a stress-strain analysis to measure in vivo cardiac mechanics has the advantage that the slope of the end-systolic stress-strain relation, systolic myocardial stiffness, is both independent of load and unaffected by the size of the heart or the extent of myocardial hypertrophy (16). Recently, we developed a method to measure simultaneous LV pressure and volume in mice using miniature piezoelectric crystals (7). To investigate whether myocardial function per se is augmented to preserve LV chamber function in the hypertrophied heart, we developed a novel method to study cardiac mechanics using a stress-strain strain analysis in the normal and hypertrophied in vivo mouse. Methodology to analyze stress-strain relations will provide a powerful tool to investigate myocardial function in vivo in genetically altered mice.

METHODS

Experimental Animals and Surgical Preparation

Wild-type DBA mice, age 14–28 wk of either sex, were used. Animals were handled according to approved protocols and animal welfare regulations of the Institutional Review Board at Duke University Medical Center. Transverse aortic constriction (TAC) was performed as previously described (17, 20).

Experimental Protocols

Determination of stress-strain relations was carried out by modifying a technique we developed to measure P-V loops in

Address for reprint requests and other correspondence: H. A. Rockman, Dept. of Medicine, Duke Univ. Medical Center, Box 3104, Durham, NC 27710 (E-mail: h.rockman@duke.edu).

The costs of publication of this article were defrayed in part by the payment of page charges. The article must therefore be hereby marked "*advertisement*" in accordance with 18 U.S.C. Section 1734 solely to indicate this fact.

the mouse (7). Before surgery, each mouse underwent noninvasive echocardiography to determine the internal chamber diameter for that animal. We previously validated the sonomicrometer technique using echocardiography and showed that it can accurately measure chamber dimensions in the in vivo mouse heart (7). Mice were then anesthetized with ketamine (100 mg/kg) and xylazine (2.5 mg/kg) and connected to a rodent ventilator after endotracheal intubation (7). Anesthesia was maintained by the administration of 0.5–1.0% isoflurane. After bilateral vagotomy, cardiac catheterization was performed with a 1.4-Fr high-fidelity micromanometer catheter inserted retrograde through the right carotid artery into the LV and a polyethylene-50 catheter placed into the left external jugular vein for dobutamine infusion (5 $\mu g \cdot kg^{-1} \cdot min^{-1}$). The chest was opened, and two pairs of miniature omnidirectional piezoelectric crystals (<0.7 mm, Sonometrics; London, Ontario, Canada) were implanted in the endocardium as follows. A purse string suture using 8-0 nylon was made on the epicardium where the crystal was to be implanted. A small incision (≈0.5 mm) on the epicardial surface in the center of the purse string was made with microdissection scissors. Each crystal was inserted into the epicardium and gently advanced to the endocardium, but not into the chamber because the rounded surface of the epoxy covering the crystal cannot pierce through the endocardial layer. The wire was then sutured with 8-0 nylon to secure the crystal. To measure instantaneous anterior wall thickness, a fifth crystal was attached on the epicardium of the anterior wall using cyanoacrylate adhesive (Vetbond, 3M Animal Care Products; St Paul, MN). Miniature piezoelectric crystals used in this study were hand made by the manufacturer to be ~0.7 mm in length and 0.5 mm in width and were attached to a 42-gauge (0.102 mm) copper wire. Proper positioning of the crystals in vivo was confirmed by comparing the readout of chamber dimensions in real time with that obtained by noninvasive echocardiography just before instrumentation. Importantly, the tip of the crystal that transmits and detects the acoustic signal lies within the endocardial layer. Total blood loss resulting from the small epicardial incision was minimal.

A suture was then placed around the transverse aorta for the transient augmentation of afterload (Fig. 1). The space and time resolution of the sonomicrometry system were 0.015 mm and 0.001 s, respectively, and three-point smoothing function was applied.

After steady-state hemodynamics were achieved, pressure and dimension measurements were taken during the increase in afterload generated by gently pulling on the suture to transiently constrict the transverse aorta. The contractile state was increased with a dobutamine infusion (2 $\mu g \cdot kg^{-1} \cdot min^{-1}$). After a steady state (~4 min) was reached, pressure and dimension measurements were repeated during the transient increase in afterload. All data were recorded digitally at 2,000 Hz and stored on computer for off-line analysis (7). At the end of each experiment, the animals were killed, and proper positioning of the crystals was documented by direct inspection.

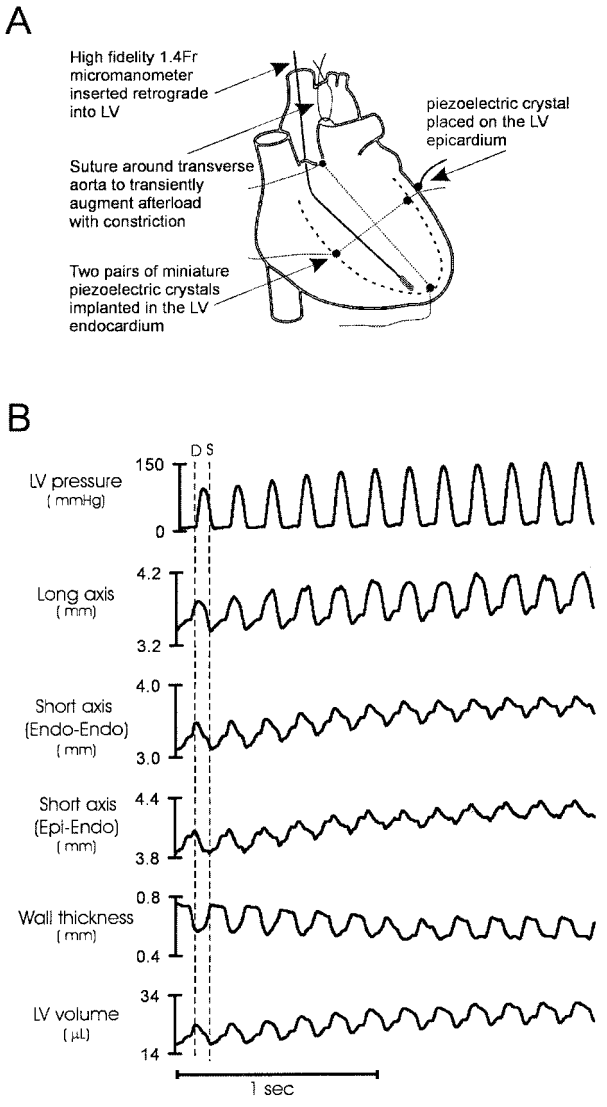

Fig. 1. *A*: schematic of the instrumented mouse heart. *B*: representative tracings from a control mouse during transient aortic constriction (TAC). Shown are the left ventricular (LV) pressure, long-axis dimension, 2 short-axis dimensions [endocardial (Endo)-Endo and Endo-epicardial (Epi)], wall thickness subtracted from 2 short-axis measurements, and calculated LV volume during transient augmentation of afterload. End-diastolic (D) and end-systolic (S) time points (dotted lines) are shown.

Data Analysis

End-systolic P-V relation. End diastole was defined as the onset of rapid upstroke of the derivative of LV pressure (LV d*P*/d*t*). End systole was defined at the point of maximal $P/(V - V_0)$ ratio, where V_0 is the volume axis intercept. LV volume was calculated as a modified general ellipsoid (12, 23). The end-systolic points were fitted to a parabolic curvilinear equation as follows: $P_{es} = a(V_{es} - V_0)^2 + b(V_{es} - V_0)$, where P_{es} is the end-systolic pressure, V_{es} is the end-systolic volume, b is the local slope at V_0 [which reflects cardiac contractility (E'_{max})], and a is the curvilinearity coefficient (12, 23). The time constant of relaxation (τ) was calculated by using a monoexponential model with nonzero asymptotic offset.

Stress-strain relations. Stress-strain relations were calculated using an ellipsoid model of LV geometry as previously described by Mirsky et al. (16). The average stress difference (σ) was calculated by $\sigma = \sigma_{\theta a} - \sigma_{ra} = PLD/2h(L + 0.55D + 1.1h) + P/2$, where $\sigma_{\theta a}$ is the average circumferential stress, σ_{ra} is approximately $-P/2$ and is the average radial stress, P is the LV pressure, and L, D, and h are the long-axis, short-axis, and LV wall thickness, respectively (16). LV wall thickness was obtained by subtracting the short-axis dimension (anterior endocardium to posterior endocardium) from the outer short-axis dimension (anterior epicardium to posterior endocardium) (Fig. 1).

Natural strain is defined as $\ln(D_m/D_{om})$, where D_m is the instantaneous midwall diameter of the LV and D_{om} is zero-stress midwall diameter. Mathematical calculation to obtain the end-systolic stress-strain relation is described as $\sigma_{es} = E_{avmax} \times K_m \ln(D_{mes}/D_{om}) = E_{avmax} \times \varepsilon_{es}$, where σ_{es} is end-systolic stress, ε_{es} is the end-systolic midwall natural strain, D_{mes} is the end-systolic midwall diameter, E_{avmax} is the maximum systolic myocardial stiffness, and $K_m = (2/3)(2 + D^2_{mes}/L^2_{mes})$, with L_m being the midwall long axis. E_{avmax} is an index of LV contractility analogous to E'_{max} and independent of loading condition, heart size, and the extent of hypertrophy.

Diastolic myocardial stiffness (E_s) is defined as $E_s = K_m d\sigma = K_m d\sigma/(dD_m/D_m) = K_m(\gamma\sigma) = k\sigma$, where $d\sigma$ is the incremental stress difference, $d\varepsilon$ ($= dD_m/D_m$) is the midwall incremental strain, and the observed stress-diameter relation during aortic constriction is curve fitted to the form ($\sigma = CD_m^{\gamma}$), where C and γ are regression coefficients. Thus the myocardial stiffness constant (k) is a dimensionless constant that represents myocardial passive diastolic properties (16).

In vivo systolic wall stress at matched afterload. After 7 days of aortic constriction, simultaneous aortic pressures of the right carotid (proximal to the stenosis) and the left axillary artery (distal to the stenosis) were measured in the anesthetized mice to obtain the systolic pressure gradient (SPG). The chest was then reopened, the suture around the transverse aorta was removed, and a new suture was placed for the transient augmentation of afterload. To compare σ_{es} at matched afterload in chronically banded mice with unbanded control mice, the in vivo σ_{es} of the afterloaded ventricle in response to TAC was estimated by adding the individual SPG to the end-systolic pressure at the basal level before TAC (21). For the unbanded control mice, the σ_{es} at matched high afterload was estimated by adding the mean SPG of the TAC mice to the end-systolic pressure at the basal level of individual control mice.

Statistical Analysis

Serial hemodynamic data between control and dobutamine treatment were analyzed using a paired Student's *t*-test. Hemodynamic data between control and TAC mice were analyzed using an unpaired Student's *t*-test. A two-way ANOVA followed by a least-significant-difference method post hoc test was used to compare wall stress in control and TAC mice. $P < 0.05$ was considered significant. All data are shown as means ± SD.

RESULTS

Systolic Function and Sensitivity to Inotropic State in Control Mice

Representative tracings of short- and long-axis dimensions and wall thickness are shown during the transient augmentation of afterload by gradual constriction of the transverse aorta in a control mouse in Fig. 1*B*. As afterload was transiently augmented, the percent wall thickening and stroke volume decreased, whereas LV end-diastolic volume was increased. Hemodynamic responses to dobutamine infusion are shown in Table 1. Significant increases in both isovolu-

Table 1. *Hemodynamic parameters in the baseline unloaded state*

	Control		
	Baseline	Dobutamine	TAC
Body weight, g	26.4 ± 7.5		25.9 ± 3.4
LV weight/body weight, mg/g	3.5 ± 0.5		5.2 ± 0.8‡
SPG, mmHg			62 ± 11
	Hemodynamics		
Heart rate, beats/min	336 ± 59	393 ± 66*	337 ± 70
LVSP, mmHg	90 ± 12	110 ± 21	82 ± 15
LVEDP, mmHg	8.7 ± 2.4	10.9 ± 1.9	6.7 ± 02.8
LV dP/dt_{max}, mmHg/s	4,115 ± 1,162	5,749 ± 954*	4,590 ± 1,256
LV dP/dt_{min}, mmHg/s	−4,150 ± 1,361	−5,259 ± 1,150*	−2,905 ± 1,097†
τ, ms	17.4 ± 7.8	11.4 ± 2.9*	23.9 ± 5.0†
	ESPVR		
LVEDV, μl	49 ± 31	42 ± 21	59 ± 15
LVEDV/body weight, μl/g	1.8 ± 0.7	1.5 ± 0.5	2.3 ± 0.7
LVESV, μl	41 ± 29	32 ± 18	50 ± 12
LVEF, %	20 ± 7	25 ± 6*	16 ± 3
a	−0.056 ± 0.170	−0.573 ± 0.756	−1.144 ± 1.352
E'_{max}, mmHg/μl	8.4 ± 3.4	18.9 ± 11.0*	24.3 ± 15.8†
V_0, μl	30 ± 23	26 ± 17	47 ± 12†
	Wall thickness		
WT_{ed}, mm	0.80 ± 0.27	0.67 ± 0.18	1.08 ± 0.19†
WT_{es}, mm	0.93 ± 0.28	0.84 ± 0.17	1.18 ± 0.19†
WT, %	18.1 ± 8.5	24.4 ± 9.5*	9.0 ± 3.9†

Data are means ± SD; $n = 7$ control mice and 13 transverse aortic constricted (TAC) mice. LV, left ventricular; SPG, systolic pressure gradient; LVSP, LV systolic pressure measured after suture removal in 7-day TAC mice; LVEDP, LV end-diastolic pressure; LV dP/dt_{max}, maximal derivative of LV pressure; LV dP/dt_{min}, minimal derivative of LV pressure; τ, time constant of LV pressure decay during the isovolumic relaxation period; ESPVR, end-systolic pressure-volume relation; LVEDV, LV end-diastolic volume; LVESV, LV end-systolic volume; LVEF, LV ejection fraction; *a*, curvilinearity coefficient of the parabolic ESPVR; E'_{max}, local slope at the volume intercept of the ESPVR (V_0); WT_{ed}, end-diastolic wall thickness; WT_{es}, end-systolic wall thickness; WT, percent wall thickening.*$P < 0.05$, baseline vs. dobutamine in control mice; †$P < 0.05$ and ‡$P < 0.01$, control (baseline) vs. TAC mice.

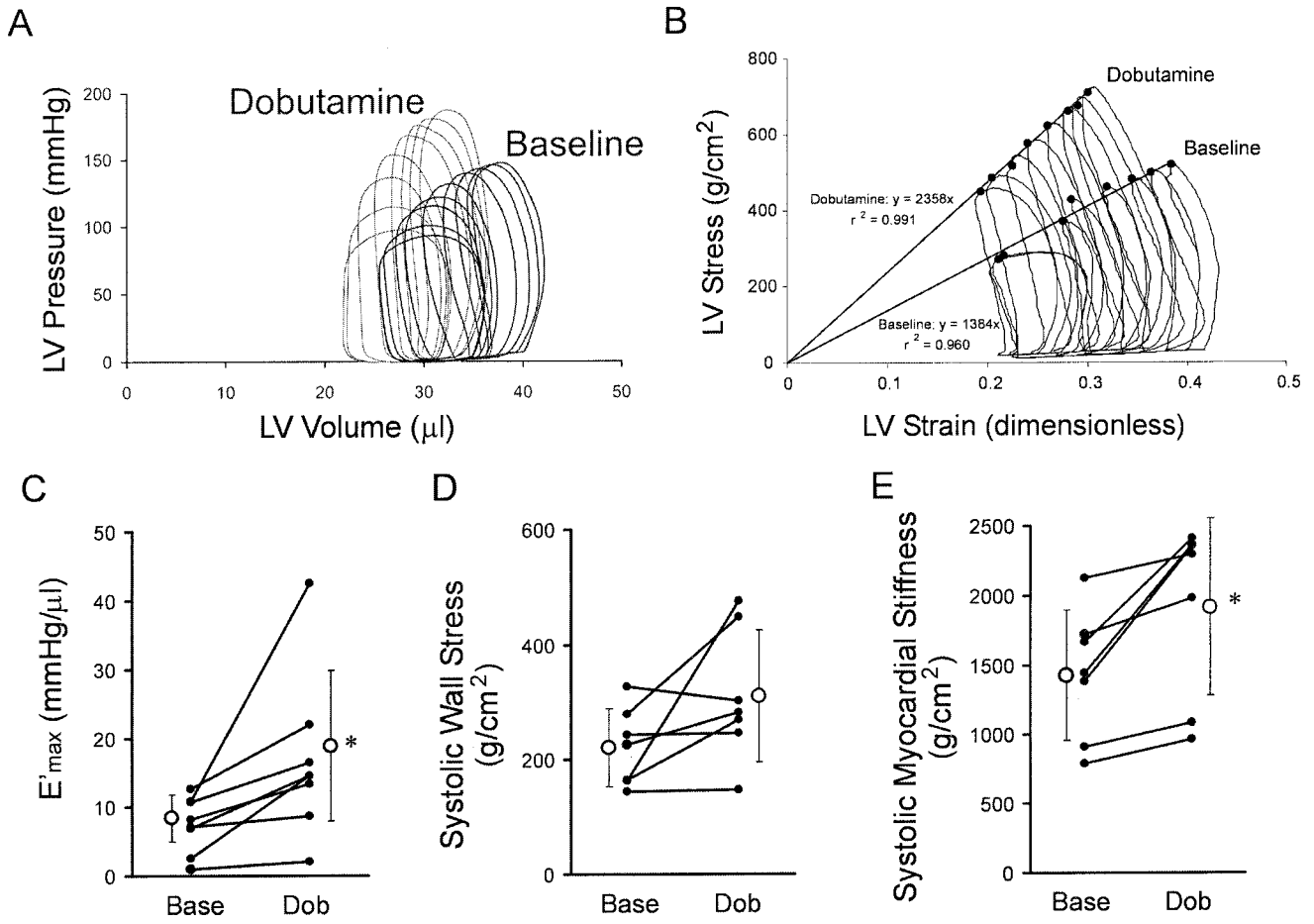

Fig. 2. *A*: representative pressure-volume loops for a control mouse. End-systolic pressure-volume relation was curvilinear, and dobutamine (Dob) shifted the pressure-volume loop left and upward. *B*: representative stress-strain tracings for a control mouse at baseline (Base) and after Dob. End-systolic stress-strain relation was linear, and Dob shifted the relation left and upward. *C–E*: systolic parameters before and after Dob in control mice (n = 7). *C*: the local slope at the volume intercept of the curvilinear end-systolic pressure-volume relation (E'_{max}) was increased with Dob, indicating an increase in myocardial contractility. *D*: systolic wall stress did not change after Dob. *E*: systolic myocardial stiffness, as assessed by the slope of the end-systolic stress-strain relation, was increased, indicating an increase in myocardial contractility. ●, Data for individual mice; ○, average of the group at each condition. *$P < 0.02$.

mic and ejection phase indexes of systolic function were observed with dobutamine. Likewise, dobutamine caused a significant decrease in LV dP/dt_{min} and the time constant of LV decay during the isovolumic relaxation period (τ).

Representative P-V and stress-strain loops for one control mouse are shown in Fig. 2, *A* and *B*. The end-systolic P-V relation was curvilinear with the mean square of the correlation coefficient (r^2) of 0.944 ± 0.005 at baseline and 0.993 ± 0.007 after dobutamine (Fig. 2*A*). Dobutamine shifted the P-V loop left and upward (Fig. 2*A*) and increased E'_{max} by 155 ± 163% (Fig. 2*C*) without altering V_0 (Table 1). Highly linear systolic stress-strain relations were obtained at baseline (r^2 = 0.978 ± 0.023) and after dobutamine (r^2 = 0.974 ± 0.030). Representative tracings are shown in Fig. 2*B*. Dobutamine shifted the stress-strain relation left and upward, indicating an increase in myocardial contractility. Although dobutamine did not change systolic wall stress (Fig. 2*D*), it increased systolic myocardial stiffness from 1,435 ± 467 to 1,923 ± 631 g/cm^2 ($P < 0.02$; Fig. 2*E*).

Systolic Function in the Mouse Heart With Pressure Overload Hypertrophy

To determine the myocardial properties of the hypertrophied mouse heart, we studied mice that underwent TAC for 7 days (Table 1). Figure 3 shows representative in vivo P-V (Fig. 3*A*) and stress-strain relations (Fig. 3*B*) for a hypertrophied heart. In Fig. 3*A* for a TAC mouse, *A* is the end-systolic pressure at baseline condition and *B* is baseline end-systolic pressure plus SPG. In Fig. 3*B*, *A′* is σ_{es} at baseline and *B′* is σ_{es} at the end-systolic pressure plus SPG. For the unbanded control mice, the σ_{es} at matched high afterload was estimated by adding the mean SPG of the TAC mice to the end-systolic pressure at the basal level of individual control mice. In Fig. 3*A* for a control mouse, *X* is the end-systolic pressure at baseline conditions and *Y* is

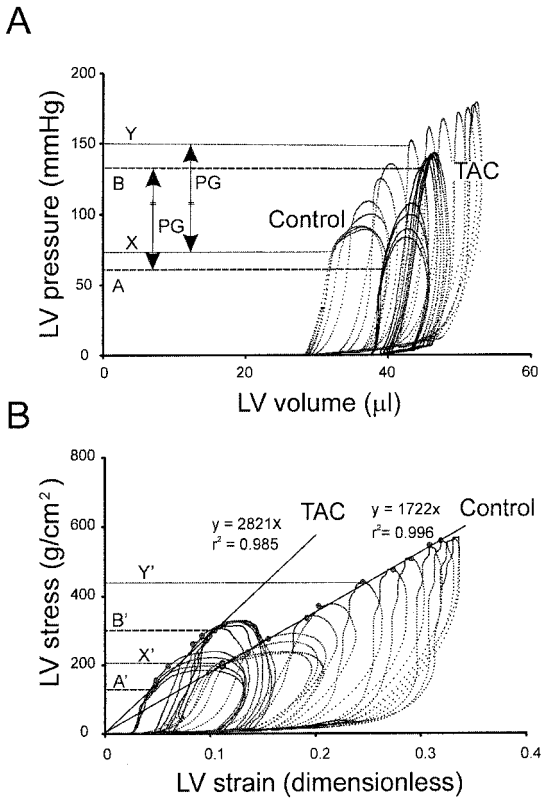

Fig. 3. Representative in vivo pressure-volume and stress-strain tracings from an unbanded control mouse and a hypertrophied mouse 7 days after TAC. *A*: end-systolic pressure-volume relation in the hypertrophied mouse was more curvilinear than that in the control mouse. *Point A*, end-systolic pressure at baseline conditions in a TAC mouse; *point B*, estimated in vivo end-systolic pressure in a TAC mouse obtained by adding the individual pressure gradient (SPG) to the baseline end-systolic pressure; *point X*, end-systolic pressure at baseline conditions in a control mouse; *point Y*, estimated in vivo end-systolic pressure at matched high afterload obtained by adding the mean SPG of the TAC mice to the baseline end-systolic pressure of each control mouse. *B*: highly linear end-systolic stress-strain relations were obtained in both control and TAC mice. *Point A′*, systolic wall stress (σ_{es}) at baseline condition in a TAC mouse; *point B′*, estimated in vivo σ_{es} at the end-systolic pressure plus SPG; *point X′*, σ_{es} at baseline conditions in a control mouse; *point Y′*, estimated in vivo σ_{es} at the estimated in vivo end-systolic pressure at matched high afterload in a control mouse. PG, pressure gradient across the TAC.

the estimated in vivo end-systolic pressure at high afterload, obtained by adding the mean SPG of the TAC mice to *X*. In Fig. 3*B*, *X′* is σ_{es} at baseline conditions in a control mouse and *Y′* is σ_{es} at the estimated in vivo end-systolic pressure plus mean SPG of TAC mice. End-systolic P-V relations of the hypertrophied mouse hearts showed greater curvilinearity than that of the control hearts, as indicated by the lower curvilinearity coefficient a (Table 1). In contrast, highly linear systolic stress-strain relations were obtained in the hypertrophied hearts ($r^2 = 0.953 \pm 0.049$).

σ_{es} at high afterload was reduced in the hypertrophied mice compared with that in control mice at matched pressure, but still higher than the σ_{es} at baseline in control mice (Fig. 4*A*). Interestingly, contractile function was significantly enhanced as shown by the higher E'_{max} (Fig. 4*B*) and greater systolic myocardial stiffness (Fig. 4*C*) in hypertrophied mice compared with the control mice.

Diastolic Function

We used the diastolic stiffness constant to assess the myocardial diastolic properties of normal and hypertrophied mouse hearts. The diastolic stiffness constant was calculated as the slope of the relation between diastolic myocardial stiffness and diastolic wall stress (Fig. 5*A*). In control mice, dobutamine increased diastolic wall stress from 23 ± 12 to 33 ± 15 g/cm^2 ($P < 0.05$; Fig. 5*B*), whereas the diastolic stiffness constant remained unchanged (Fig. 5*C*). In contrast, the development of cardiac hypertrophy with TAC resulted in marked abnormalities in diastolic function, as shown by an increase in both τ (Table 1) and the diastolic stiffness constant (Fig. 5*C*), without a significant change in diastolic wall stress compared with unbanded controls (Fig. 5*B*).

DISCUSSION

In this study, we investigated the mechanical properties of the normal and hypertrophied mouse heart. To this end, we applied a novel method to assess instantaneous wall stress and strain in the in vivo mouse heart. We showed that, in adult mice, highly

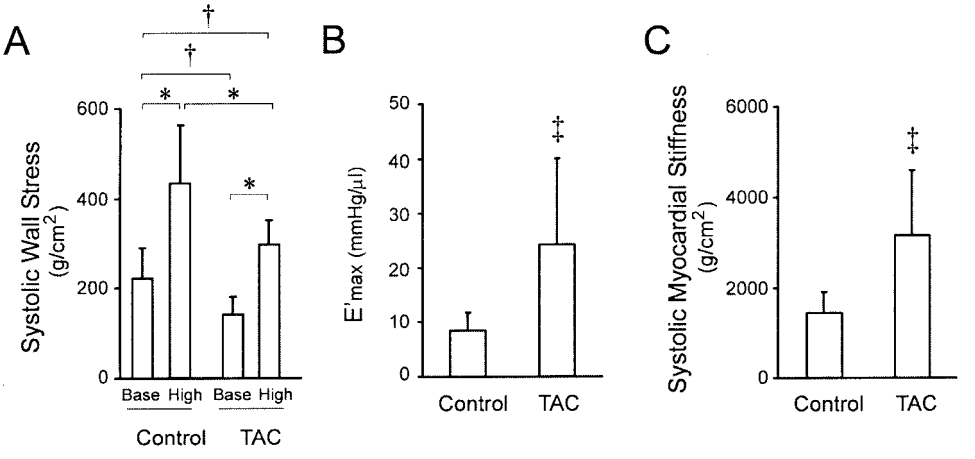

Fig. 4. Comparison of systolic parameters between control ($n = 7$) and TAC mice ($n = 13$). *A*: systolic wall stress at high afterload (High) in the hypertrophied heart was significantly lower than the estimated wall stress at high afterload in control mice but still significantly greater than at basal conditions. Indexes of myocardial contractility are shown. *B*: E'_{max}. *C*: systolic myocardial stiffness was significantly higher in TAC than control mice. *$P <$ 0.01, High vs. Base for either control or TAC mice; †$P < 0.05$, Base TAC or High TAC vs. Base control; ‡$P < 0.05$, control vs. TAC mice.

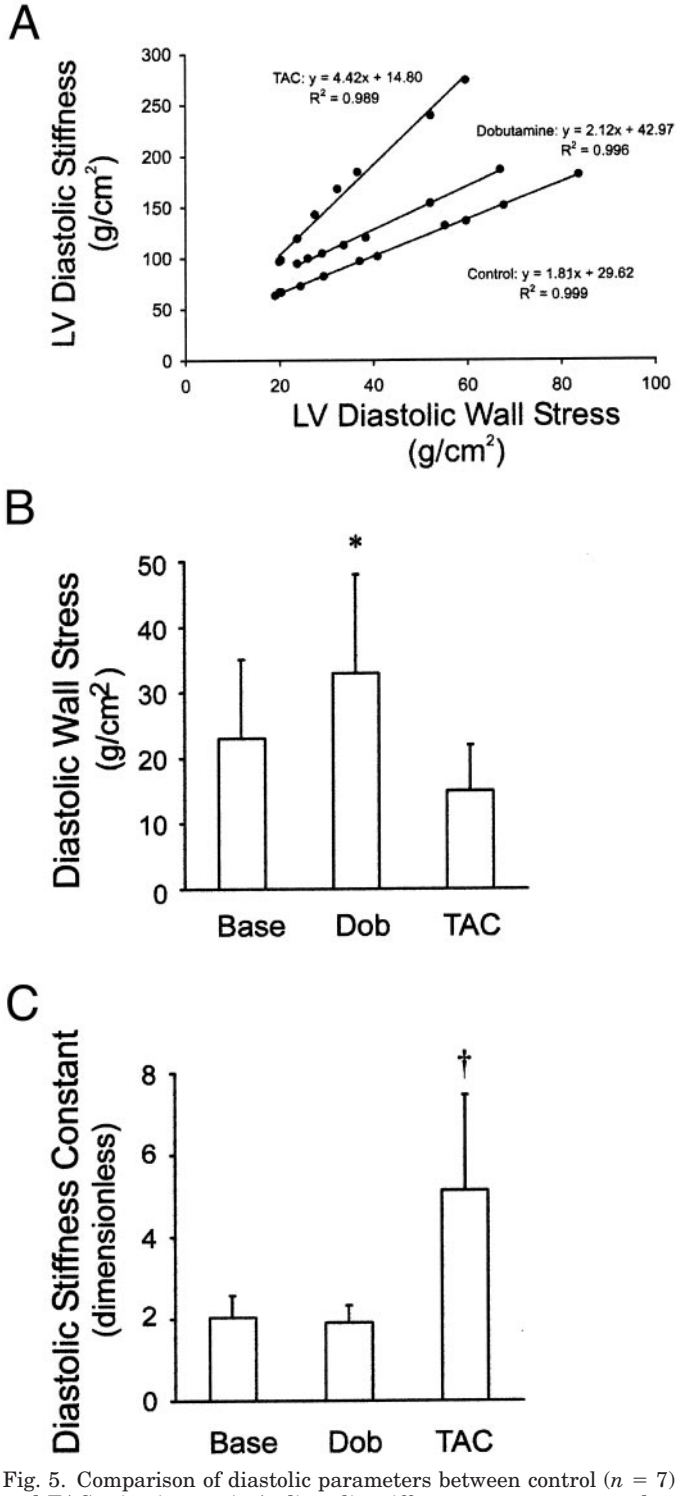

Fig. 5. Comparison of diastolic parameters between control ($n = 7$) and TAC mice ($n = 13$). *A*: diastolic stiffness constant was used to assess the myocardial diastolic properties and was calculated as the slope of the relation between diastolic myocardial stiffness and diastolic wall stress. Representative examples for a mouse from each of the 3 groups are shown. *B*: diastolic wall stress showed no difference between control and TAC mice at baseline but was increased after Dob infusion in control mice. *C*: diastolic stiffness constant remained unchanged after Dob infusion in control mice but was significantly higher in mice after TAC, indicating an impaired passive diastolic property. *$P < 0.05$, Base or TAC vs. Dob; †$P < 0.01$, Base or Dob vs. TAC.

Table 2. *Comparisons of cardiac mechanics in different species*

Animal	Wall Stress, g/cm²		Systolic Stiffness, g/cm²	Diastolic Stiffness Constant	E'_{max}, mmHg/ml
	Systolic	Diastolic			
Dog	162 ± 17	18 ± 8	1,781 ± 469	3.1 ± 0.3*	2.7 ± 1.0
Human	320 ± 23	25 ± 5		13.9 ± 3.7	3.2 ± 1.3
Mouse	222 ± 26	23 ± 5	1,435 ± 177	2.0 ± 0.2	8,400 ± 1,300

Data shown are means ± SD (*means ± SE). Data for the dog are from Refs. 3, 13, 16, and 26; data for the human are from Refs. 11, 19, and 25; and data for the mouse are from the present study.

linear stress-strain relations can be obtained in vivo and the slope of the stress-strain relation, systolic myocardial stiffness, is a sensitive measure of LV contractility. Furthermore, our results show that the myocardial contractile state in the hypertrophied heart might be augmented, perhaps as an early compensatory response to pressure overload despite only partial normalization of wall stress.

Stress-Strain Analysis in the In Vivo Murine Heart

While LV dP/dt_{max} is useful to detect relative changes in contractility in the same animal, it is less reliable to detect differences in intrinsic contractility between groups of animals (4, 15). In this regard, one of the best measures of cardiac contractile function in vivo is the P-V loop (12, 23). Indeed, in our studies, LV dP/dt_{max} was not different between TAC and control groups, whereas both E'_{max} and systolic myocardial stiffness parameters showed a state of enhanced contractility in the pressure-overloaded hypertrophied ventricle. The inability of LV dP/dt_{max} to detect changes in intrinsic contractility between groups of pathological mice is similar to the result found with cardiac-targeted expression of the β-adrenergic receptor kinase-1 inhibitor (βARKct), which we showed to rescue the muscle LIM protein$^{-/-}$ heart failure phenotype (7).

Although E'_{max} is a powerful and established tool to evaluate the LV contractile state, it has limitations because of the dependence on heart size and the extent of hypertrophy (18, 21). For example, in young and old dogs, E'_{max} was found to be dependent on ventricular size by a logarithmic function, whereas systolic myocardial stiffness was nearly constant (18). The concept of end-systolic stress-strain relation and systolic myocardial stiffness is useful in the evaluation of LV function because the slope of the relation is load independent and, importantly, the slope is not affected by the size of the heart. Systolic myocardial stiffness is described mathematically as the change in stress ($d\sigma$) divided by the change in strain ($d\epsilon$) and reflects the myocardial contractile state. Because genetically altered mice may show a variety of cardiac phenotypes including LV hypertrophy with or without LV chamber dilatation, the application of the systolic stress-strain analysis would be especially suited to assess intrinsic myocardial function in gene-targeted and transgenic mice.

We compared systolic myocardial stiffness among different species to support its independence on heart size (Table 2). Myocardial systolic stiffness in the mouse heart is comparable to that in the dog at ≈1,500 g/cm^2. Moreover, systolic and diastolic wall stress for the mouse heart is similar to that measured in the dog (3, 13, 16, 26) and even human heart (11, 19). In contrast, because the size of the mouse heart is considerably smaller, E'_{max} in the mouse is much higher than in either dogs (16, 26) or humans (25). These data demonstrate that the underlying myocardial properties are conserved across a broad range of mammalian species and underscore the utility of this method to study cardiac mechanics in the in vivo open-chest mouse.

Myocardial Function in the Hypertrophied Heart

It is interesting that we document hyperfunction of the hypertrophied heart. This is consistent with a previous study showing enhanced LV contractility in the presence of elevated wall stress in a rat model of severe hypertension (6). Sasayama et al. (21) also reported that the LV end-systolic pressure-diameter relation was shifted to the left in conscious unsedated dogs after 2.5 wk of aortic banding, indicating enhanced function, whereas the wall stress-diameter relation was not shifted. They interpreted these results as hyperfunction with a lack of change in myocardial contractility. In contrast to our results, other studies have suggested that the hypertrophied ventricle has diminished contractility (5, 14, 22). This discrepancy may, in part, be attributed to the difference in the duration or the extent of pressure overload or to a species difference.

Limitations

The measurement of stress-strain relations using the sonomicrometer technique requires open-chest instrumentation, which is technically demanding and will affect the measurement of basal hemodynamic parameters. The combination of open-chest measurements with the need to implant miniature piezoelectric crystals through the wall of the LV influences the contractile state of the heart. Proper alignment of the crystals placed on the endocardium and epicardium of the anterior free wall is important to obtain wall thickness. Proper alignment of the endocardial crystals is also important to measure the true short axis of the cardiac chamber. In this study, careful attention to the location of the crystals was performed before and after each experiment. Proper positioning of the crystals in vivo was confirmed by comparing the readout of chamber dimensions in real time with that obtained by noninvasive echocardiography just before instrumentation. Post mortem, correct positioning of the crystals was determined by removing the heart and opening the chamber at the level of the crystals. If either the endocardium-endocardium or endocardium-epicardium crystals were positioned incorrectly, the data were not analyzed. Therefore, we view this load- and heart size-independent method to evaluate intrinsic contractile state of the mouse as complementary to that of closed-chest- and conductance catheter-based hemodynamic (8) and echocardiography (10) measurements. In addition, it is important to measure LV function under the same open-chest conditions for all experimental groups when assessing the dependence on loading condition and heart size in genetically engineered mice, as was done in this study.

Finally, the potential for myocardial ischemia due to crystal placement is possible, which was easily detected because the time-wall thickness curves show systolic bulging. In this study, the time-wall thickness curve in one mouse demonstrated systolic bulging and therefore was not included in the analysis.

This work was supported by National Heart, Lung, and Blood Institute Grants HL-56687 and HL-46345. H. A. Rockman was the recipient of a Burroughs Wellcome Fund Clinical Scientist Award in Translational Research.

REFERENCES

1. **Adams JW, Sakata Y, Davis MG, Sah VP, Wang Y, Liggett SB, Chien KR, Brown JH, and Dorn GW II.** Enhanced Galphaq signaling: a common pathway mediates cardiac hypertrophy and apoptotic heart failure. *Proc Natl Acad Sci USA* 95: 10140–10145, 1998.
2. **Akhter SA, Luttrell LM, Rockman HA, Iaccarino G, Lefkowitz RJ, and Koch WJ.** Targeting the receptor-Gq interface to inhibit in vivo pressure overload myocardial hypertrophy. *Science* 280: 574–577, 1998.
3. **Aoyagi T, Fujii AM, Gelpi RJ, Hittinger L, Crocker VM, and Mirsky I.** Application of the systolic stiffness concept to assess myocardial function in developing hypertension. *Jpn Heart J* 31: 71–85, 1990.
4. **Davidson DM, Covell JW, Malloch CI, and Ross J Jr.** Factors influencing indices of left ventricle contractility in the conscious dog. *Cardiovasc Res* 8: 299–312, 1974.
5. **De Simone G, Devereux RB, Celentano A, and Roman MJ.** Left ventricular chamber and wall mechanics in the presence of concentric geometry. *J Hypertens* 17: 1001–1006, 1999.
6. **De Simone G, Devereux RB, Volpe M, Camargo MJ, Wallerson DC, and Laragh JH.** Relation of left ventricular hypertrophy, afterload, and contractility to left ventricular performance in Goldblatt hypertension. *Am J Hypertens* 5: 292–301, 1992.
7. **Esposito G, Santana LF, Dilly K, Cruz JD, Mao L, Lederer WJ, and Rockman HA.** Cellular and functional defects in a mouse model of heart failure. *Am J Physiol Heart Circ Physiol* 279: H3101–H3112, 2000.
8. **Georgakopoulos D and Kass D.** Minimal force-frequency modulation of inotropy and relaxation of in situ murine heart. *J Physiol* 534: 535–545, 2001.
9. **Grossman W, Jones D, and McLaurin LP.** Wall stress and patterns of hypertrophy in the human left ventricle. *J Clin Invest* 56: 56–64, 1975.
10. **Harding VB, Jones LR, Lefkowitz RJ, Koch WJ, and Rockman HA.** Cardiac beta ARK1 inhibition prolongs survival and augments beta blocker therapy in a mouse model of severe heart failure. *Proc Natl Acad Sci USA* 98: 5809–5814, 2001.
11. **Hood WP Jr, Rackley CE, and Rolett EL.** Wall stress in the normal and hypertrophied human left ventricle. *Am J Cardiol* 22: 550–558, 1968.
12. **Kass DA, Beyar R, Lankford E, Heard M, Maughan WL, and Sagawa K.** Influence of contractile state on curvilinearity of in situ end-systolic pressure-volume relations. *Circulation* 79: 167–178, 1989.
13. **Komamura K, Shannon RP, Pasipoularides A, Ihara T, Lader AS, Patrick TA, Bishop SP, and Vatner SF.** Alter-

ations in left ventricular diastolic function in conscious dogs with pacing-induced heart failure. *J Clin Invest* 89: 1825–1838, 1992.
14. **Liu CP, Ting CT, Lawrence W, Maughan WL, Chang MS, and Kass DA.** Diminished contractile response to increased heart rate in intact human left ventricular hypertrophy. Systolic versus diastolic determinants. *Circulation* 88: 1893–1906, 1993.
15. **Mahler F, Ross J Jr, O'Rourke RA, and Covell JW.** Effects of changes in preload, afterload and inotropic state on ejection and isovolumic phase measures of contractility in the conscious dog. *Am J Cardiol* 35: 626–634, 1975.
16. **Mirsky I, Tajimi T, and Peterson KL.** The development of the entire end-systolic pressure-volume and ejection fraction-afterload relations: a new concept of systolic myocardial stiffness. *Circulation* 76: 343–356, 1987.
17. **Naga Prasad SV, Esposito G, Mao L, Koch WJ, and Rockman HA.** Gbetagamma-dependent phosphoinositide 3-kinase activation in hearts with in vivo pressure overload hypertrophy. *J Biol Chem* 275: 4693–4698, 2000.
18. **Nakano K, Sugawara M, Ishihara K, Kanazawa S, Corin WJ, Denslow S, Biederman RW, and Carabello BA.** Myocardial stiffness derived from end-systolic wall stress and logarithm of reciprocal of wall thickness. Contractility index independent of ventricular size. *Circulation* 82: 1352–1361, 1990.
19. **Peterson KL, Tsuji J, Johnson A, DiDonna J, and LeWinter M.** Diastolic left ventricular pressure-volume and stress-strain relations in patients with valvular aortic stenosis and left ventricular hypertrophy. *Circulation* 58: 77–89, 1978.
20. **Rockman HA, Ross RS, Harris AN, Knowlton KU, Steinhelper ME, Field LJ, Ross J Jr, and Chien KR.** Segregation of atrial-specific and inducible expression of an atrial natriuretic factor transgene in an in vivo murine model of cardiac hypertrophy. *Proc Natl Acad Sci USA* 88: 8277–8281, 1991.
21. **Sasayama S, Franklin D, and Ross J Jr.** Hyperfunction with normal inotropic state of the hypertrophied left ventricle. *Am J Physiol Heart Circ Physiol* 232: H418–H425, 1977.
22. **Shimizu G, Zile MR, Blaustein AS, and Gaasch WH.** Left ventricular chamber filling and midwall fiber lengthening in patients with left ventricular hypertrophy: overestimation of fiber velocities by conventional midwall measurements. *Circulation* 71: 266–272, 1985.
23. **Suga H.** Ventricular energetics. *Physiol Rev* 70: 247–277, 1990.
24. **Suga H, Sagawa K, and Shoukas AA.** Load independence of the instantaneous pressure-volume ratio of the canine left ventricle and effects of epinephrine and heart rate on the ratio. *Circ Res* 32: 314–322, 1973.
25. **Takaoka H, Takeuchi M, Odake M, Hayashi Y, Hata K, Mori M, and Yokoyama M.** Comparison of hemodynamic determinants for myocardial oxygen consumption under different contractile states in human ventricle. *Circulation* 87: 59–69, 1993.
26. **Wolff MR, de Tombe PP, Harasawa Y, Burkhoff D, Bier S, Hunter WC, Gerstenblith G, and Kass DA.** Alterations in left ventricular mechanics, energetics, and contractile reserve in experimental heart failure. *Circ Res* 70: 516–529, 1992.